applied optics

Intercomparison of bidirectional reflectance distribution function measurements at in- and out-of-plane geometries

N. Basic,[1,*] E. Molloy,[2] A. Koo,[2] A. Ferrero,[3] P. Santafé Gabarda,[3] L. Gevaux,[4] G. Porrovecchio,[5] A. Schirmacher,[6] M. Šmíd,[5] P. Blattner,[1] K.-O. Hauer,[6] T. Quast,[6] J. Campos,[3] and G. Obein[4]

[1]Eidgenössisches Institut für Metrologie METAS, Bern-Wabern, Switzerland
[2]MSL Measurement Standards Laboratory of NZ, Callaghan Innovation, Lower Hutt, New Zealand
[3]Instituto de Óptica "Daza de Valdés," Consejo Superior de Investigaciones Científicas, Madrid, Spain
[4]LNE-CNAM (EA 2367), La Plaine St. Denis, France
[5]Cesky Metrologicky Institut (CMI), Brno, Czech Republic
[6]Physikalisch-Technische Bundesanstalt, Braunschweig, Germany
*nina.basic@metas.ch

Received 25 January 2023; revised 20 March 2023; accepted 21 March 2023; posted 22 March 2023; published 21 April 2023

In recent years, there has been a growing interest in the measurements of the bidirectional reflectance distribution function (BRDF) in industry and research and development. However, there is currently no dedicated key comparison to demonstrate the scale conformity. To date, scale conformity has been proved only for classical in-plane geometries, in comparisons between different national metrology institutes (NMIs) and designated institutes (DIs). This study aims at expanding that with nonclassical geometries, including, for the first time, to the best of our knowledge, two out-of-plane geometries. A total of four NMIs and two DIs participated in a scale comparison of the BRDF measurements of three achromatic samples at 550 nm in five measurement geometries. The realization of the scale of BRDF is a well-understood procedure, as explained in this paper, but the comparison of the measured values presents slight inconsistencies in some geometries, most likely due to the underestimation of measurement uncertainties. This underestimation was revealed and indirectly quantified using the Mandel–Paule method, which provides the interlaboratory uncertainty. The results from the presented comparison allow the present state of the BRDF scale realization to be evaluated, not only for classical in-plane geometries, but also for out-of-plane geometries.

https://doi.org/10.1364/AO.486156

1. INTRODUCTION

Requests for quantitative measurements of visual appearance have substantially increased in recent years because of their value in industry as customers place increasing importance on the aesthetic appeal of merchandise. More and more complex materials developed by industry require measurements of the so-called bidirectional reflectance distribution function (BRDF) [1], where one measures how a material reflects light when illuminated from a given direction. These measurements play an important role in optical metrology applications [2] and aerospace projects, as well as in many industries, such as automotive [3], paper, textile, color, cosmetics, 3D printing [4], high-technology, and virtual reality.

Consequently, new commercial multi-angle and bidirectional spectrophotometers have been developed. Typically, they are relative measuring devices that require traceability to the absolute reflectance scale maintained at dedicated national metrology institutes (NMIs) and designated institutes (DIs) via diffuse reflectance standards. NMIs must continue supporting development in spectrophotometry by providing bidirectional reflectance calibration services for angular configurations other than the classical (0°, 0°) : (45°, 0°) and (45°, 0°) : (0°, 0°) configurations, defined in terms of spherical coordinates (see also Section 2.A).

Bidirectional reflectance scales are currently not included in any key comparison arranged by the Consultative Committee of Photometry and Radiometry (CCPR) of the International Committee for Weights and Measures (CIPM), but bilateral comparisons were conducted, e.g., the one between the National Institute of Standards and Technology (NIST) and the Physikalisch-Technische Bundesanstalt (PTB) for (0°, 0°) : (45°, 0°) geometry [5]. Another comparison was conducted between a total of six NMIs and DIs (Germany, Finland, Spain, New Zealand, Sweden, and France) for (0°, 0°) : (45°, 0°) and (45°, 0°) : (0°, 0°) geometries within an European Metrology

Research Programme (EMRP) project [6]. However, both comparisons focused only on classical in-plane geometries.

This paper presents a multilateral scale comparison of BRDF measurements performed between the following NMIs and DIs: Eidgenössisches Institut für Metrologie (METAS, Switzerland), Consejo Superior de Investigaciones Científicas (CSIC, Spain), Measurement Standards Laboratory (MSL, New Zealand), Conservatoire National des Arts et Métiers (LNE-CNAM, France), Physikalisch-Technische Bundesanstalt (PTB, Germany), and Cesky Metrologicky Institut (CMI, Czech Republic). The comparison was performed on three achromatic samples at 550 nm in five measurement geometries, including, for the first time, two out-of-plane geometries.

2. MEASUREMENTS

A. Measurement Protocol

The measurement comparison included two nominally identical sample sets (#1 and #2), which consisted of three achromatic samples: two sintered polytetrafluoroethylene (PTFE) samples and one satin sample. The two PTFE samples, provided by Labsphere [7], had nominal reflectance values of 99% and 50%. They were identified as PTFE99 and PTFE50. The satin sample was produced specifically for the measurement comparison by Natural Colour System (NCS) [8]. The sample consisted of white acrylic paint spread by pulverization on a glass substrate to provide good support and ensure the sample's flatness and stability. In contrast to the two PTFE samples, the satin sample was not a quasi-Lambertian sample: it had a nominal gloss value of 20 GU at 60° measurement geometry [9]. The satin sample was identified as Satin20. All samples were 5 cm by 5 cm squares with a clear indication of orientation, which allowed for easy alignment of the sample with respect to the illumination angle for the measurements.

Set #1 was used for the round robin comparison and set #2 was kept as a reference at METAS, which served as the pilot. Both sets were measured at METAS at the start and finish of the measurement comparison to check the stability of the samples and the variation between the sample sets.

Each participant measured the samples in five measurement geometries: three in-plane and two out-of-plane geometries (Table 1). The geometries are defined in terms of spherical coordinates as $(\theta_i, \varphi_i) : (\theta_r, \varphi_r)$, where θ_i is the incidence polar angle, φ_i the incidence azimuthal angle, θ_r the reflection polar angle, and φ_r the reflection azimuthal angle, all expressed in degrees (Fig. 1). The origin for the azimuth angles is physically realized in the samples, and it corresponds to $\varphi_i = 0°$.

The (45°, 0°) : (0°, 0°) and (0°, 0°) : (45°, 180°) geometries were selected based on their widespread use and their recommendation both by Commission Internationale de l'Eclairage (CIE) [10] and American Society for Testing and Materials

Table 1. Measurement Geometries Used in the Comparison

	Geometries $(\theta_i, \varphi_i) : (\theta_r, \varphi_r)$
In-plane	(45°, 0°) : (0°, 0°)
	(0°, 0°) : (45°, 180°)
	(45°, 0°) : (60°, 180°)
Out-of-plane	(45°, 0°) : (45°, 90°)
	(45°, 0°) : (50.1°, 146.6°)

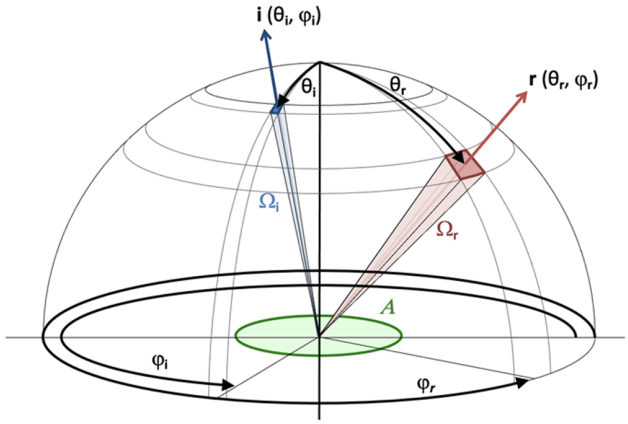

Fig. 1. Description of geometry notation. Also marked are the measurement area A and the two solid angles Ω_i and Ω_r.

(ASTM) [11,12]. The (45°, 0°) : (60°, 180°) measurement geometry was selected as one of the recommended ones by ASTM [11]. The closeness to the specular direction allowed us to check the alignment of the setups, since any variation in the alignment produces large variation in the BRDF value, especially for the Satin20 sample. Figure 2 is showing the in-plane BRDF values for the three samples illuminated at (45°, 0°) with unpolarized light of 550 nm. There is no recommendation concerning out-of-plane geometries; therefore, inspiration was taken from commercial multi- angle spectrophotometers, and two specific geometries were chosen according to the last entries in Table 1.

B. Description of the Measurand and Measurement Methods

The measurand for the comparison is the BRDF [1] of a 10 mm diameter area in the center of each sample in the above-defined five geometries for unpolarized light of 550 nm with a 5 nm bandwidth. The parameters were carefully selected in order to avoid any polarization bias [13] or speckle influence [14,15]. The decision of conducting the comparison at only one wavelength is supported by the flatness of the spectra for all three samples, as seen in Fig. 3.

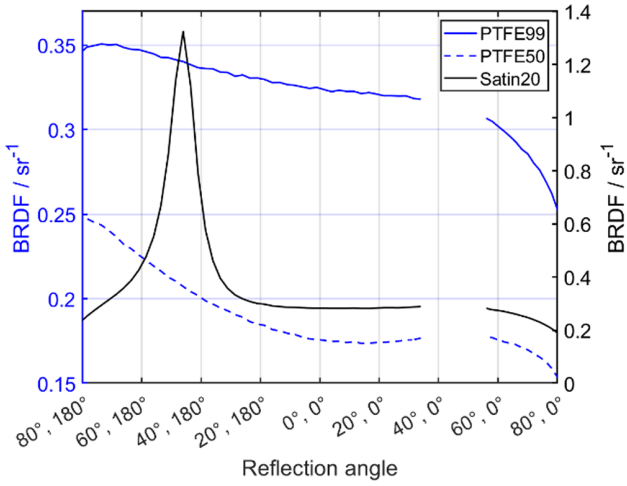

Fig. 2. In-plane angular characteristics of the samples illuminated at (45°, 0°) using unpolarized light of 550 nm.

The BRDF is defined as the ratio of the reflected radiance L_r from the surface to the irradiance E_i on it [16],

$$f_r(\theta_i, \varphi_i, \theta_r, \varphi_r, \lambda) = \frac{L_r(\theta_i, \varphi_i, \theta_r, \varphi_r, \lambda)}{E_i(\theta_i, \varphi_i, \lambda)}. \quad (1)$$

In the above equation, λ represents the wavelength of the light. For fluorescent materials, the incident and reflected wavelengths may differ. The samples chosen for the comparison are nonfluorescent; hence, we continue using the same wavelength for both the incidence and reflection direction.

There are two absolute methods for measuring BRDF: the over-illumination method and the under-illumination method. They differ in how they illuminate the sample. For the over-illumination method, one needs to provide a uniform irradiance over the entire sample and measure the radiance of the sample. In this case, the BRDF is given as [16]

$$f_r = \frac{L_r}{L_i} \frac{(R_i^2 + r_i^2)}{\pi r_i^2 \cos\theta_i}, \quad (2)$$

where L_i is the light source's radiance, R_i the distance from the light source aperture to the sample surface, and r_i is the radius of a circular light source aperture. A different equation holds for the under-illumination method, where a relatively small spot on the sample is illuminated and one measures the amount of light scattered into a known solid angle [16],

$$f_r = \frac{\Phi_r}{\Phi_i} \frac{(R_r^2 + r_r^2)}{\pi r_r^2 \cos\theta_r}, \quad (3)$$

where Φ_r is the reflected radiant flux, Φ_i the incident radiant flux, R_r the distance from the detector aperture to the sample surface, and r_r is the radius of a circular detector aperture.

The relative method for measuring BRDF makes use of a reference sample with a known BRDF, $f_{r,ref}$, calibrated elsewhere [16],

$$f_r = \frac{L_r}{L_{ref}} f_{r,ref}, \quad (4)$$

where L_{ref} is the radiance scattered from the reference sample in the same geometry as the sample.

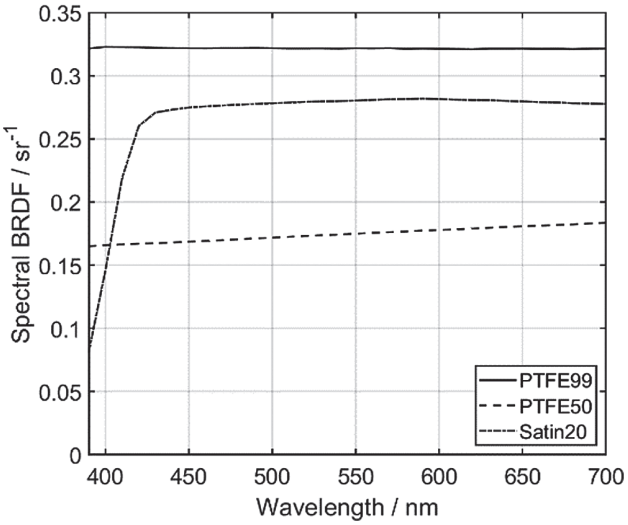

Fig. 3. Spectral reflection characteristics of the samples at (45°, 0°) : (0°, 0°).

C. Description of Measurement Facilities

An overview of the basic parameters of the measurement facilities participating in the measurement comparison is presented in Table 2, together with a few measurement parameters that differ, depending on the facility. The description of each facility is presented in the following text, while their schematics are gathered in Fig. 4.

The instrument at METAS [Fig. 4(a)] performs relative measurements using a reference sample with traceability to PTB. The illumination is quasi-monochromatic using a commercially available tunable light source with a wavelength range of 390 nm up to 700 nm. A Köhler optical system ensures that the sample is illuminated uniformly with a quasi-collimated beam. The detector is a CCD camera with an integrated filter wheel, which can be used to directly measure the chromaticity coordinates when used together with a broadband light source (LDLS) instead of a tunable one.

The Gonio-EspectroFotómetro Español (GEFE) goniospectrophotometer [Fig. 4(b)] of CSIC [17,18] performs relative measurements using as a reference a (0°, 0°) : (45°, 0°) reflectance standard calibrated absolutely at CSIC by an absolute method with under-illumination. The instrument has a fixed irradiation system, the sample is mounted on a robot arm, and the detection unit is placed on a ring on a platform rotating around the robot arm. In order to irradiate the samples uniformly and with an almost collimated beam, a long Köhler optical system is used. For the absolute method, an LDLS is used in combination with a single monochromator for providing

Table 2. Basic Parameters of the Measurement Facilities with Some Measurement Parameters

	Solid Angle (sr)			Spectral Determination Method		
Participant	Illumination	Detection	Measurement Method	Source	Detection	Irradiation Polarization
METAS	0.0019	0.00025	Relative[a]	Quasi-monochromatic	Broadband	Unpolarized
CSIC	0.001	0.006	Relative[b]	Broadband	Monochromatic	Unpolarized
CMI	0.0002	0.0011	Absolute	Monochromatic	Broadband	Unpolarized
PTB	0.0022	0.00012	Absolute	Broadband	Monochromatic	Unpolarized
MSL	<0.00010	0.0030	Absolute	Monochromatic	Broadband	Polarized
CNAM	0.00018	0.0010	Absolute	Monochromatic	Broadband	Unpolarized

[a]Relative to 45°:0° realization at PTB.
[b]Relative to 0°:45° realization at CSIC.

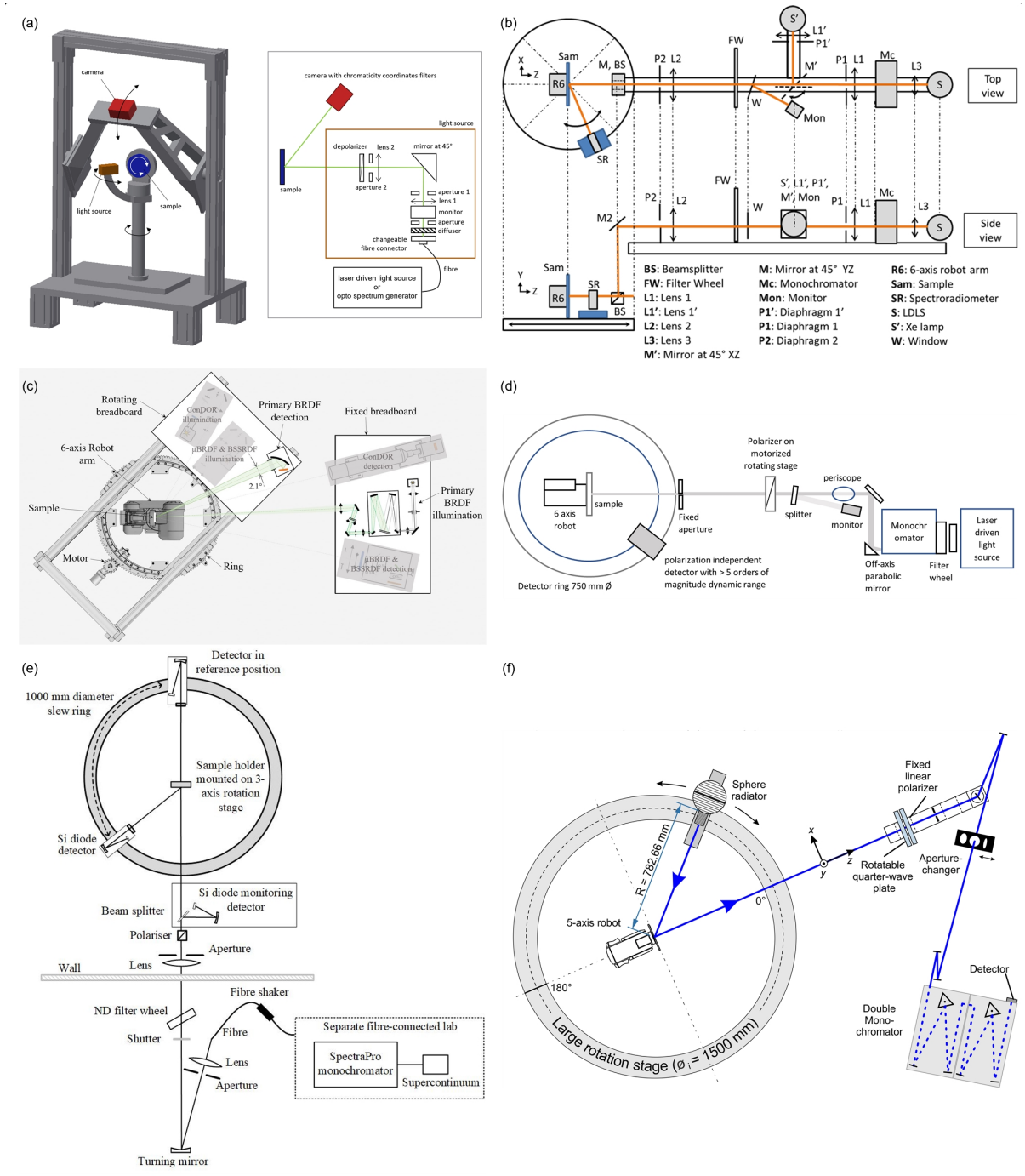

Fig. 4. Schematics of measurement facility at (a) METAS, (b) CSIC, (c) CNAM, (d) CMI, (e) MSL, and (f) PTB.

monochromatic irradiation. In the case of the relative method, a Xenon lamp is used for broadband illumination and a spectroradiometer (Konica–Minolta CS-2000 A) is used for detection in the visible range (380–780 nm), with a spectral bandwidth between 4 and 5 nm.

The instrument at CMI [Fig. 4(d)] comprises a six-axis robot arm to hold the sample and a motorized ring to rotate the detection system. The monochromatic illumination is provided by a broadband high-intensity LDLS coupled with a monochromator with a spectral bandwidth of 5 nm. The optical output from the monochromator is then collimated to illuminate the sample by an off-axis parabolic mirror and set to the proper alignment with the sample by a beam steerer. The illumination polarization is controlled by a linear film polarizer mounted on a motorized rotation stage. The polarization-independent detection system, developed in cooperation with MSL [19], is composed of an aperture, a mirror, and a low-noise silicon photodiode mounted on a small integrating sphere. The light passing through the aperture of 17 mm diameter is collected by the mirror and reimaged at the input port of the integrating

sphere. The photodiode's photocurrent is transformed into a voltage signal by a switched integrator amplifier developed by CMI [20] with a dynamic range up to 5 orders of magnitude.

The goniospectrophotometric calibration facility at PTB [Fig. 4(f)] is described in detail in [21,22]. This system applies a radiator-based approach in which the solid angle of the illuminating source determines the radiance factor. An unpolarized homogenous sphere radiator [23] is rotated around the sample on a ring mount. Sample manipulation is performed by a five-axis robot system. In combination with a fixed detection direction, almost any geometry can be used for measurements. The detection is performed with a double-monochromator system and by applying a quarter-wave plate linear polarizer combination, which delivers a full polarization analysis in terms of the Stokes parameters.

In the instrument at MSL [Fig. 4(e)], the sample is mounted on a three-axis rotation stage positioned in the center of a slew ring, which the detector rotates around. A Köhler optical system illuminates the sample with collimated and polarized light from a supercontinuum source coupled to a monochromator with a 1.5 nm bandwidth. The stability of the source is monitored throughout the measurements. The radiance of the sample is detected using a silicon photodiode detector without further wavelength or polarization filtering. Measurements are made with vertically and horizontally polarized incident light, then averaged to obtain the BRDF for unpolarized light.

The CNAM goniospectrophotometer [Fig. 4(c)] performs absolute measurements in an under-illumination configuration. It is composed of an illumination unit on a fixed table, a six-axis robot arm, which acts as the sample holder, and a detection unit that can be rotated around the robot arm on a ring with a diameter of 1.1 m. For illumination, a quartz tungsten halogen (QTH) filament is focused on the entrance slit of a single monochromator with a bandwidth of 5 nm. The light exiting the monochromator is modulated by an optical chopper and goes through an optical system designed to image a diaphragm on the sample plane with a magnification of 2. Any partial polarization created by the gratings is removed by a Lyot depolarizer. The detection is made of a combination of a silicon photodiode and a lock-in amplifier.

D. Methodology of the Comparison

The evaluation of the measurement comparison follows the Guidelines for CCPR Key Comparison Report Preparation using the Mandel–Paule method [24,25]. It starts with the BRDF value f_n for each participant (indexed by n) and its standard uncertainty $u(f_n)$. In total, there were six participants. METAS acted as the pilot and measured the samples at the beginning and end of the comparison. The METAS values used in the comparison analysis are the average of these two measurements. The reported uncertainties of each participant are adjusted by the cutoff value,

$$u_{\mathrm{cut}}(f_n) = u(f_n) \quad \text{for } u(f_n) \geq u_{\mathrm{cut-off}}$$
$$u_{\mathrm{cut}}(f_n) = u_{\mathrm{cut-off}} \quad \text{for } u(f_n) < u_{\mathrm{cut-off}}. \tag{5}$$

The cutoff value is calculated as

$$u_{\mathrm{cut-off}} = \mathrm{average}\{u(f_n)\}$$
$$\text{for } u(f_n) \leq \mathrm{median}\{u(f_n)\}; \quad n = 1:N, \tag{6}$$

where N is the number of participants—six in the case of this comparison. A provisional reference value R for every sample and measurement geometry is calculated using the weighted mean as

$$R = \sum_{n=1}^{N} w_n f_n, \tag{7}$$

where the weights w_n are determined as

$$w_n = \frac{u_{\mathrm{cut}}^{-2}(f_n)}{\sum_{n=1}^{N} u_{\mathrm{cut}}^{-2}(f_n)}. \tag{8}$$

The uncertainty of the reference value is given by

$$u(R) = \sqrt{\sum_{n=1}^{N} u^2(f_n) w_n^2}. \tag{9}$$

The next step is to check the consistency of the data by calculating the chi-square value χ^2_{obs},

$$\chi^2_{\mathrm{obs}} = \sum_{n=1}^{N} \frac{(f_n - R)^2}{u^2(f_n)}. \tag{10}$$

The data is regarded consistent if it passes the chi-square test $\chi^2_{\mathrm{obs}} \leq \chi^2_{0.05}(N-1)$. The values $\chi^2_{0.05}(N-1)$ are taken from the reference table that can be found in [24]. If the data are not consistent and there are no apparent outliers, the uncertainty is adjusted by applying an interlaboratory variance s^2,

$$u_{\mathrm{adj}}(f_n) = \sqrt{u^2(f_n) + s^2}. \tag{11}$$

The newly adjusted uncertainty is used to replace the $u(f_n)$ in Eqs. (5)–(10) and the value s is determined by an iterative process until the data set passes the above-mentioned chi-square test. The iterative process is executed for every sample and every geometry separately. Once the data are regarded as consistent, the provisional values from Eqs. (7) and (9) are taken as definitive reference values and their uncertainties, and the unilateral degrees of equivalence (DoEs) and their corresponding uncertainties are calculated as

$$\mathrm{DoE}_n = \frac{f_n - R}{R} \tag{12}$$

$$u(\mathrm{DoE}_n) = 2\sqrt{\frac{u^2(f_n)}{R^2} + \frac{u^2(R) f_n^2}{R^4} - 2\frac{u^2(f_n) w_n f_n}{R^3}}. \tag{13}$$

The reader should notice that the effect of correlation between the participants' measurements and the reference value is taken into account in the above-defined uncertainty.

3. RESULTS AND DISCUSSION

Figure 5 depicts the measured BRDF values along with the reported expanded uncertainties. The three samples exhibit different angular distributions. PTFE99 is the most diffuse of

the three, having a relatively small difference between the (45°, 0°) : (0°, 0°) (diffuse) and (45°, 0°) : (60°, 180°) (near-specular) geometry. Although PTFE50 shows angular distribution similar to PTFE99, we can see that it is less diffuse compared to PTFE99, since the difference between (45°, 0°) : (0°, 0°) and (45°, 0°) : (60°, 180°) geometry is larger. The different angular distributions of the two PTFE samples measured here are in agreement with a BRDF study of the gray-scale Spectralon [26]. In contrast, Satin20 is semi-glossy, with a high BRDF value for the near-specular (45°, 0°) : (60°, 180°) geometry and almost constant BRDF value for the rest of the geometries.

The selection of the combination of samples and geometries allows us to identify any systematic errors in the measurements, especially concerning the alignment of angles and sample alignment. The (45°, 0°) : (0°, 0°) and (0°, 0°) : (45°, 180°) geometries provide a baseline for the diffuse part, while the rest of the geometries show the variation in the BRDF value and are, therefore, more susceptible to any alignment error.

It has to be noted that the variation in participants' measurements shown in the graphs is larger than the variation of the sample measurements performed at the beginning and end of the comparison. Therefore, we can exclude any sample related issue from the following discussion.

A. Compatibility Index for (0°, 0°) : (45°, 180°) and (45°, 0°) : (0°, 0°)

The BRDF values for (45°, 0°) : (0°, 0°) and (0°, 0°) : (45°, 180°) are expected to have the same values for isotropic samples, since these two geometries are interchangeable according to the Helmholtz reciprocity principle [27]. However, the samples used in the comparison are not necessarily isotropic. To test how nonisotropic the samples are, we calculated the compatibility index C_n between (45°, 0°) : (0°, 0°) and (0°, 0°) : (45°, 180°) geometries for every participant separately as

$$C_n = \frac{\left| f_n(0°,\ 45°) - f_n(45°,\ 0°) \right|}{\sqrt{\left\{2u[f_n(0°,\ 45°)]\right\}^2 + \left\{2u[f_n(45°,\ 0°)]\right\}^2}}. \quad (14)$$

The measurements are compatible when the C_n index is lower than 1. The calculated indices are gathered in Table 3. They show very good compatibility between the two geometries, with only one value above 1, meaning that the samples are isotropic. However, the PTFE50 and Satin20 have slightly higher indices than PTFE99. A possible explanation for this may be some anisotropy in these samples, which might be caused by a slightly bowl-shaped surface topology for PTFE50 and waviness of the surface for the Satin20, as seen in Fig. 6.

B. Uncertainty Components

The reference value is computed using the Mandel–Paule method, where an interlaboratory uncertainty component s is added to all participants' uncertainties until $\chi^2_{\text{obs}} = \chi^2_{0.05}(5) = 11.070$, as described above. The iterative process is executed for every sample and every geometry separately. Table 4 gathers the s values, while Fig. 7 shows the reported expanded relative

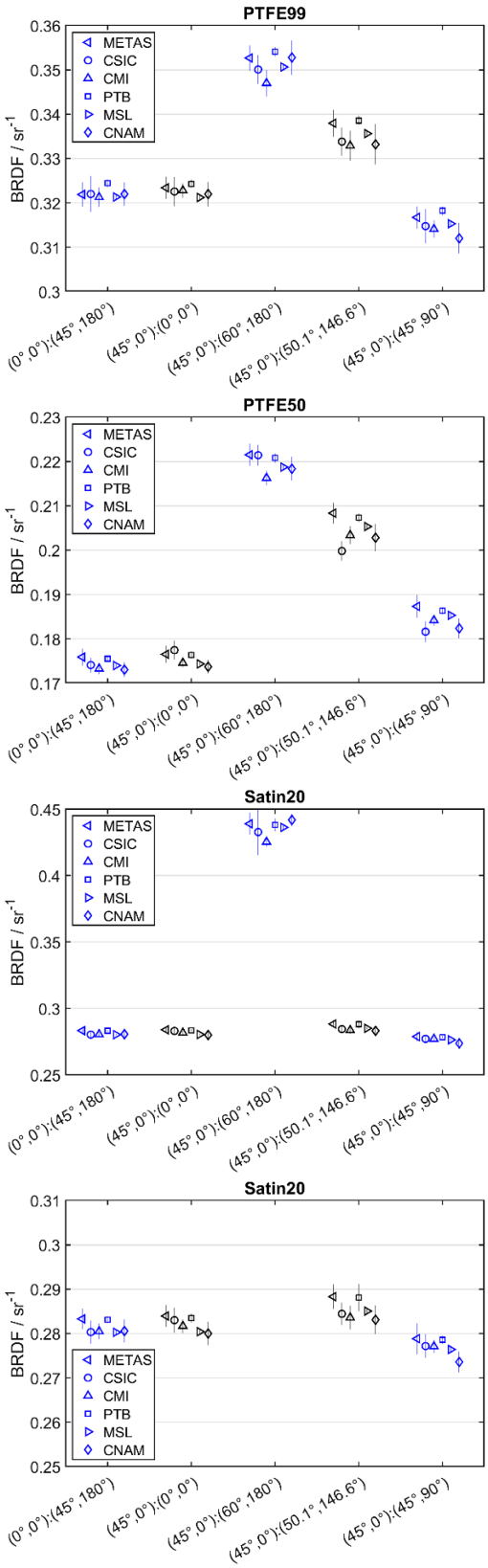

Fig. 5. Measured BRDF values (markers) along with the reported expanded ($k = 2$) uncertainties (bars). The Satin20 sample is represented in two different scales in order to better show the values at all measurement geometries. See Data File 1 for underlying values.

Table 3. Compatibility Index C_n between (0°, 0°) : (45°, 180°) and (45°, 0°) : (0°, 0°)

Participant	PTFE99	PTFE50	Satin20
METAS	0.41	0.23	0.20
CSIC	0.11	1.20	0.70
CMI	0.55	0.81	0.51
PTB	0.08	0.84	0.32
MSL	0.13	0.81	0.19
CNAM	0.01	0.28	0.15

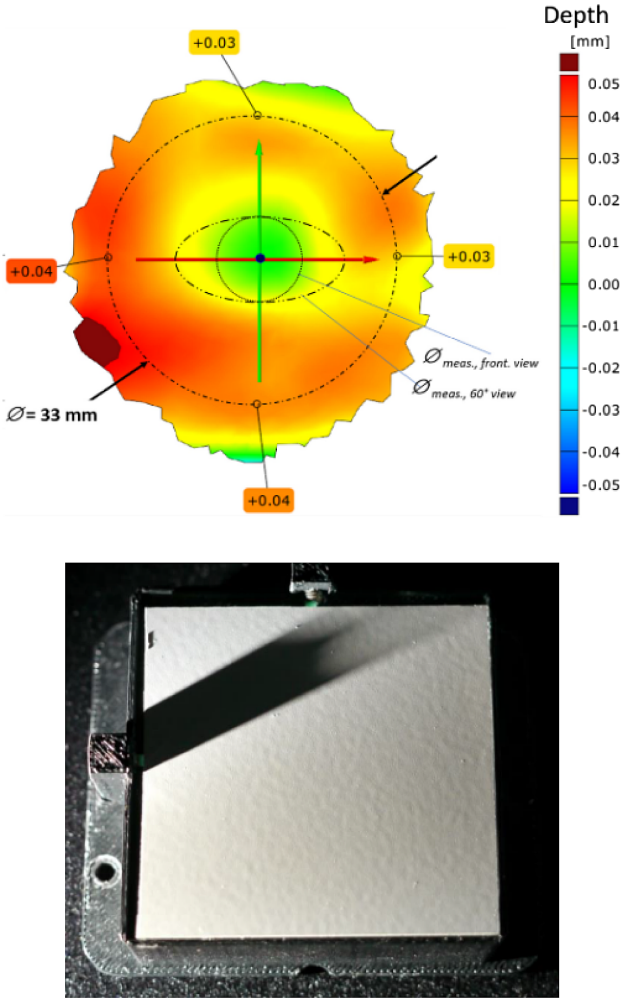

Fig. 6. False color image of surface topology of PTFE50 (top) and photograph of Satin20 illuminated at grazing incidence (bottom).

Table 4. Interlaboratory Uncertainty Component $s \times 10^{-4}$ sr^{-1}

Measurement Geometry	PTFE99	PTFE50	Satin20
(45°, 0°) : (0°, 0°)	6.0	4.3	6.6
(0°, 0°) : (45°, 180°)	5.5	6.6	7.3
(45°, 0°) : (60°, 180°)	12	10	32
(45°, 0°) : (50.1°, 146.6°)	9.5	11	7.3
(45°, 0°) : (45°, 90°)	11	18	4.4

uncertainties in comparison to the adjusted expanded relative uncertainties.

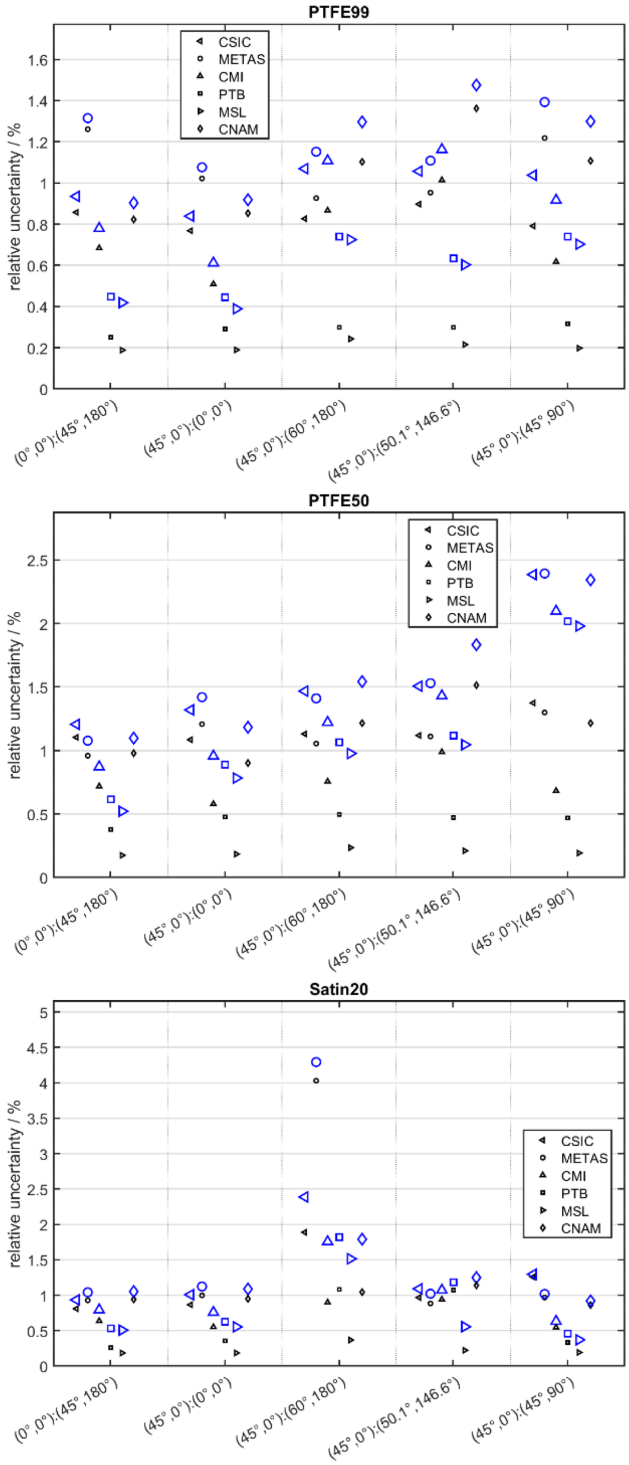

Fig. 7. Reported expanded ($k = 2$) relative uncertainties (black markers) together with adjusted expanded ($k = 2$) relative uncertainties (blue markers).

The values with the lowest reported uncertainties are affected the most by adding the s component. Consequently, this means that MSL's and PTB's uncertainties have the largest difference between the adjusted and the reported uncertainty.

For PTFE99 and PTFE50, the s component is lowest for the two classical geometries [(45°, 0°) : (0°, 0°) and (0°, 0°) : (45°, 180°)], which are the most used geometries. The rest

of the geometries have a slightly higher, but almost constant, s component for PTFE99, while that does not hold true for PTFE50. The s component for the latter sample is higher than for PTFE99 with the highest value at out-of-plane near-specular geometry [(45°, 0°) : (50.1°, 146.6°)]. On the other hand, Satin20 has low s component values for all geometries, except for the near-specular one [(45°, 0°) : (60°, 180°)].

There is no straightforward explanation for the interlaboratory uncertainty component for the (45°, 0°) : (0°, 0°) and (0°, 0°) : (45°, 180°) geometries. One possible explanation could be underestimation of the uncertainties, especially from MSL and PTB. Table 5 shows an overview of the uncertainty contributions taken into account by each participant. There does not seem to be a vital uncertainty contribution missing from any participant; it is more likely that the contributions from some participants are simply underestimated.

The requirement of adding an interlaboratory component at other geometries can be explained by disregarded setup/sample alignment issues, with a consequent underestimation of the uncertainty in some cases. The geometries with the highest s are the ones that are affected the most by the misalignment. In the Satin20 case, that is the one geometry near the specular peak–(45°, 0°) : (60°, 180°). The rest of the geometries are far enough from the specular peak not to be affected by the misalignment. Although the two PTFE samples could be regarded as semi-Lambertian, they still do exhibit a specular peak. The PTFE99 has a smaller and broader specular peak than PTFE50, which means that the selected geometries are not affected as much by the misalignment. On the other hand, the PTFE50 sample has a specular peak that is larger and narrower than the one from PTFE99, but not as narrow as that for the Satin20 sample. This means that the majority of the selected geometries are affected by the misalignment. Consequently, this explains the high s component values.

It is not surprising that the highest s value is for Satin20, for (45°, 0°) : (60°, 180°) geometry. Looking at Fig. 7, we can see that the reported uncertainties are higher than for any other sample/geometry, meaning that the uncertainty contributions concerning the alignment are taken into account. However, they seem to be underestimated. These uncertainty contributions should be revised by all participants. In particular, it might be important to quantify the uncertainty due to nonnegligible solid angles at those geometries for which the angular gradient of the BRDF can be high enough to affect the measurement.

C. Degrees of Equivalence

Figure 8 shows the relative DoEs) for all samples, together with their expanded uncertainties. The distribution of the DoEs follows the same trend as the interlaboratory uncertainty component. The DoE values are lowest for the PTFE99 for the classical geometries. The largest values are seen for the PTFE50, while Satin20 exhibits large DoEs, mainly for the near-specular geometry.

The two participants with the smallest reported uncertainties were expected to have their DoEs relatively close. However, the average DoE/$2u$(DoE) for PTB is 1.44 and for MSL it is −0.63. Surprisingly, they have the closest value for the Satin20 sample at the geometry (45°, 0°) : (60°, 180°), where the spread

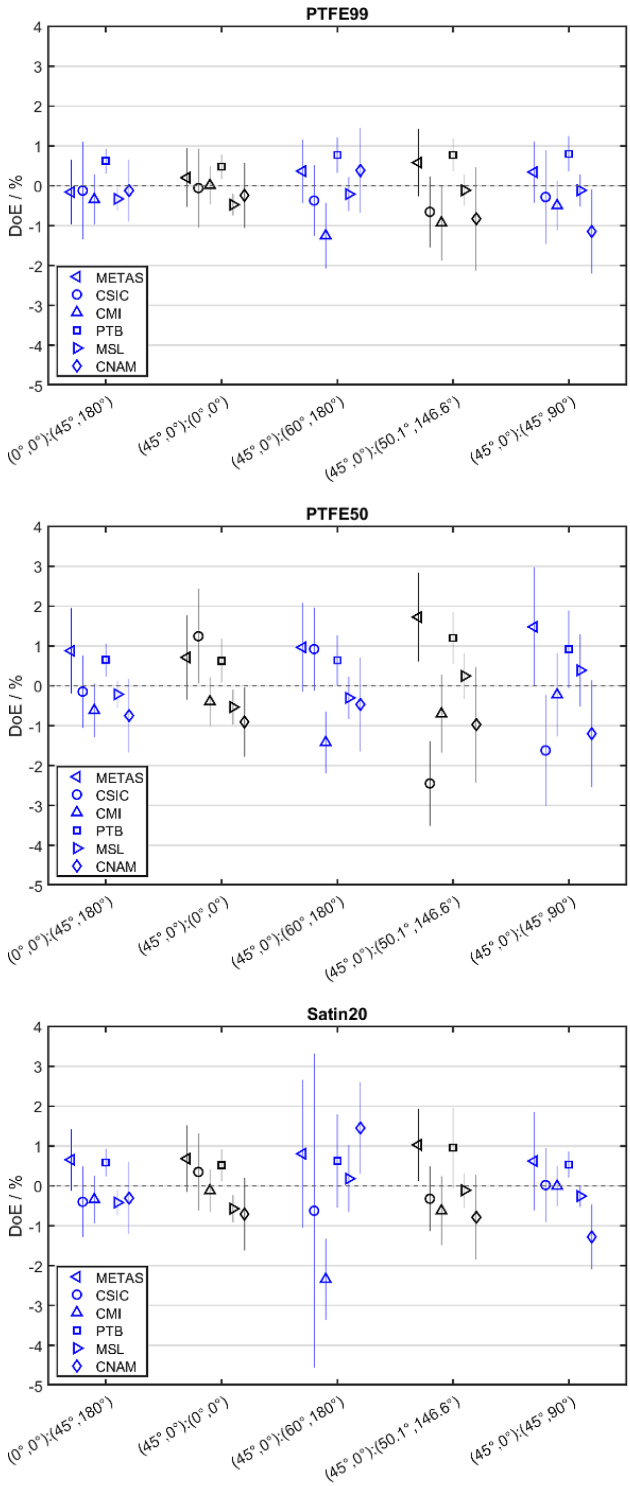

Fig. 8. Overview of the relative DoEs for all samples. See Data File 2 for underlying values.

of the DoEs is the largest. There is a trend in the data for the METAS and PTB values to be high relative to the other participants. It is not surprising the DoEs for METAS and PTB are similar, because the METAS scale is traceable to PTB. The uncertainty from the reference is one of the largest components in the METAS uncertainty budget, making their results highly

Table 5. Overview of Uncertainty Contributions Taken into Account by Each Participant

	METAS	CSIC	CMI	PTB	MSL	CNAM
Setup alignment	+	+	+	+	+	+
Solid angle calculation	N/A	N/A	+	+	+	+
Detector linearity	−	+	+	+	+	+
Gain ratio	−	N/A	+	+	+	N/A
Signal noise	+	+	+	+	+	+
Stray light	−	−	−	+	+	−
View factor	+	−	+	+	+	−
Wavelength	+	+	+	+	+	−
Polarization	+	+	−	+	+	−
Reproducibility	+	+	+	+	−	+
Reference BRDF	+	+	N/A	N/A	N/A	N/A

correlated to PTB. Note that this correlation has not been taken into account in the analysis.

The distribution of the DoEs is similar for most samples and geometries, with a few significant deviations. This suggests that the differences between the scales are systematic and cannot be explained by alignment issues alone. The differences could easily be related to other factors, such as stray light, estimates of the solid angle, and dark currents. A more detailed analysis of the uncertainty contributions should be made to understand the origin of the differences.

4. CONCLUSION

The paper presented the results of a multilateral measurement comparison of BRDF in three in-plane geometries, and for the first time, also in two out-of-plane geometries. Six participants (METAS, CSIC, CMI, PTB, MSL, and CNAM) took part in the comparison on three achromatic samples at 550 nm. The results demonstrated some discrepancies between the measurement scales. A nonnegligible contribution of interlaboratory uncertainty was estimated to achieve consistency. The most probable cause for the discrepancies is the underestimation of the alignment uncertainty contributions.

Comparing the results presented here with the previous measurement comparison [6], one can notice that PTB's values were higher than MSL's at (45°, 0°) : (0°, 0°) geometry in both comparisons. In the previous comparison performed on different sample types, PTB's values were 0.3% to 0.5% and 0.5% to 0.7% higher than MSL's for the diffuse white and diffuse light gray samples, respectively, depending on the geometry. The difference is larger in the presented study, with PTB's values being 0.96% higher than MSL's for PTFE99 and 1.2% higher than MSL's for PTFE50. On the other hand, both PTB and MSL have decreased their uncertainties since the last comparison. Further study is required to understand the origin of the difference.

In the absence of a key comparison on BRDF measurements, the presented comparison provided useful information to compare participants' scales, not only for classical geometries, but also for out-of-plane geometries.

Funding. European Metrology Programme for Innovation and Research [18SIB03 (BxDiff)].

Acknowledgment. This work has been done in the frame of the EMPIR project 18SIB03 (BxDiff) that has received funding from the EMPIR programme co-financed by the participating states and from the European Union's Horizon 2020 Research and Innovation Programme.

Disclosures. The authors declare no conflicts of interest.

Data availability. Data underlying the results presented in this paper are not publicly available at this time but may be obtained from the authors upon reasonable request.

REFERENCES AND NOTES

1. F. E. Nicodemus, J. C. Richmond, J. J. Hsia, I. W. Ginsberg, and T. Limeris, "Geometrical considerations and nomenclature for reflectance," NBS MN_160 (National Bureau of Standards, 1977).
2. See, e.g., the scientific EU-funded programs xDReflect (https://xdreflect.eu), BiRD (https://birdproject.eu), and BxDiff (https://bxdiff.cmi.cz/).
3. R. Ď. Mihálik and A. Mihalik, "Modeling the BRDF from spectral reflectance measurements of metallic surfaces," Appl. Surf. Sci. **312**, 87–90 (2014).
4. O. Rouiller, B. Bickel, J. Kautz, W. Matusik, and M. Alexa, "3D-printing spatially varying BRDFs," IEEE Comput. Graph. Appl. **33**, 48–57 (2013).
5. C. C. Cooksey, M. E. Nadal, D. W. Allen, K.-O. Hauer, and A. Höpe, "Bidirectional reflectance scale comparison between NIST and PTB," Metrologia **54**, 4006–4015 (2015).
6. C. Strothkämper, A. Ferrero, A. Koo, P. Jaanson, G. Ged, G. Obein, S. Källberg, J. Audenaert, F. B. Leloup, F. M. Martínez-Verdú, E. Perales, A. Schirmacher, and J. Campos, "Multilateral spectral radiance factor scale comparison," Appl. Opt. **56**, 1996–2006 (2017).
7. Labsphere, https://www.labsphere.com/.
8. NCS Natural Colour System, https://ncscolour.com/.
9. ISO, "Paints and varnishes: determination of gloss value at 20 degrees, 60 degrees and 85 degrees," ISO 2813:2014 (2014).
10. E. C. Carter, J. D. Schanda, R. Hirschler, S. Jost, M. R. Luo, M. Melgasa, Y. Ohno, M. R. Poynter, D. C. Rich, F. Viénot, L. Whitehead, and J. H. Wold, "Colorimetry," CIE 015:2018 (CIE, 2018).
11. ASTM, "Standard practice for multiangle color measurement of interference pigments," ASTM E2539-08 (ASTM International, 2008).
12. ASTM, "Standard guide for selection of geometric conditions for measurement of reflection and transmission properties of materials," ASTM E179-96 (ASTM International, 1996).
13. A. Calderon, A. Ferrero, and J. Campos, "Accounting for polarization–related effects in the measurement of the bidirectional reflectance distribution function," Metrologia **57**, 045003 (2020).
14. P. Chavel, M. Hébert, L. Simonot, T. Labardens, A.-M. Rabal-Almazor, and G. Obein, "Advocating a statistical definition for the BRDF," J. Phys. Conf. Ser. **2149**, 012013 (2021).
15. T. Labardens, P. Chavel, Y. Sortais, M. Hébert, L. Simonot, A. Rabal, and G. Obein, "Study and simulations of speckle effects on BRDF

measurements at very high angular resolution," in *IS&T International Symposium on Electronic Imaging* (2021).
16. J. C. Zwinkels, T. A. Germer, and B. K. Tsai, eds., "Spectrophotometry: accurate measurement of optical properties of materials," in *Experimental Methods in the Physical Sciences* (Elsevier, 2014), pp. 2–533..
17. A. M. Rabal, A. Ferrero, J. Campos, J. L. Fontecha, A. Pons, A. Rubiñoo, and A. Corróns, "Automatic gonio-spectrophotometer for the absolute measurement of the spectral BRDF at in- out-of-plane and retroreflection geometries," Metrologia **49**, 213–223 (2012).
18. B. Bernad, A. Ferrero, A. Pons, M. L. Hernanz, and J. Campos, "Upgrade of goniospectrophtometer GEFE for near-field scattering and fluorescence radiance measurements," Proc. SPIE **9398**, 93980E (2015).
19. A. Koo, G. Porrovecchio, and M. Smid, "Optical detection system for monochromatic beam goniospectrophotometry," in *4th CIE Expert Symposium on Colour and Visual Appearance*, Prague, Czech Republic, 2016.
20. J. Mountford, G. Porrovecchio, M. Smid, and R. Smid, "Development of a switched integrator amplifier for high-accuracy optical measurement," Appl. Opt. **47**, 5821–5828 (2008).
21. I. Santourian, T. Quast, and A. Schirmacher, "Uncertainty budget for PTB's gonioreflectometers and ways to improve it in the short VIS spectral range," Metrologia **59**, 025004 (2022).
22. D. Hünerhoff, U. Grusemann, and A. Höpe, "New robot-based gonioreflectometer for measuring spectral diffuse reflection," Metrologia **43**, S11 (2006).
23. A. Schirmacher, T. Quast, and K.-O. Hauer, "Polarisationseffekte in gonioreflektorischen Messungen-Untersuchungen einer Auswahl verschiedener Proben," presented at the DfwG-Jahrestagung 2016, Hanover, Germany, October 4–6, 2016, pp. 14–22.
24. G. Stokes, "2019 guidelines for CCPR key comparison report preparation," CCPR-G2 Rev.4, (CCPR, 2019).
25. R. C. Paule and J. Mandel, "Consensus values and weighting factors," J. Res. Nat. Bur. Stand. **87**, 377–385 (1982).
26. G. T. Georgiev and J. J. Butler, "BRDF study of gray-scale Spectralon," Proc. SPIE **7081**, 708107 (2008).
27. G. Stokes, "On the perfect blackness of the central spot in Newton's rings, and on the verification of Fresnel's formulae for the intensities of reflected and refracted rays," in *Mathematical and Physical Papers*, Cambridge Library Collection–Mathematics (2010), pp. 89–103.